# Second-harmonic electron-cyclotron resonance heating: A possible impact from mode coupling near the resonance

Maxim Tereshchenko [*]

*Prokhorov General Physics Institute of the Russian Academy of Sciences, 119991 Moscow, Russia*

(Received 7 February 2023; revised 20 March 2023; accepted 26 April 2023; published 17 May 2023)

The short-wavelength paraxial asymptotic technique, known as Gaussian beam tracing, is extended to the case of two linearly coupled modes in plasmas with resonant dissipation. The system of amplitude evolution equations is obtained. Apart from purely academic interest, this is exactly what happens near the second-harmonic electron-cyclotron resonance if the microwave beam propagates almost perpendicularly to the magnetic field. Because of non-Hermitian mode coupling, the strongly absorbed extraordinary mode may partly transform into the weakly absorbed ordinary mode near the resonant absorption layer. If this effect is significant, it could impair the well-localized power deposition profile. The analysis of parameter dependencies gives insight into what physical factors affect the power exchange between the coupled modes. The calculations show a rather small impact of non-Hermitian mode coupling on the overall heating quality in toroidal magnetic confinement devices at electron temperatures above 200 eV.

DOI: 10.1103/PhysRevE.107.055209

## I. INTRODUCTION

Electron cyclotron resonance heating (ECRH) is certainly one of the principal plasma heating methods in magnetic confinement systems. ECRH, as well as any plasma-wave interaction process, is a collection of various physical phenomena. A short list includes microwave beam propagation in an inhomogeneous plasma, resonant gyroaveraged electron dynamics under microwave action in an inhomogeneous magnetic field, decorrelation of electron gyrophases relative to the wave phase between the successive electron transits across the beam, and collisional relaxation of the perturbed electron velocity distribution. In spite of all intrinsic complexity, the essential features of various ECRH scenarios, such as the microwave preferable direction, polarization, and the absorption efficiency, are well described by the hot Maxwellian plasma dispersion tensor alone [1–4]. Thus, it is known that the effective second harmonic ECRH in medium-sized toroidal devices implies that mainly the fast extraordinary ($X$) mode should propagate in the plasma volume [in large devices the scenario employing the ordinary ($O$) mode also may be operative [5,6]]. Once the mixed-mode microwave beam crosses the resonance layer, where the wave frequency is nearly twice the gyrofrequency, at electron temperatures above a few hundred eV, the $X$ mode power fraction is almost completely absorbed. In experiments, this place is usually located in the plasma core. At the same time, for example at densities $\sim 10^{19}$ m$^{-3}$ and electron temperatures $\sim$1 keV, the $O$ mode power fraction loses only $\sim$10% in this layer. After the first pass through the plasma, the unabsorbed remainder of the microwave beam reflects back off the curved inner chamber wall (in the absence of a special reflector) and mostly becomes a stray radiation, whose subsequent absorption in the plasma is far from being located centrally. It can lead to an excessively wide ECRH power deposition profile, which is sometimes observed in experiments [7,8].

There can be several reasons why the $X$ mode power may be partly lost on its way from the launching structure to the plasma core, even when geometric optics predicts proper beam propagation. First, the optimal polarization (generally, elliptical) of the injected microwave notably depends on the angle between the ambient magnetic field and the wave vector at the place where the beam enters the plasma. Thus, small tuning errors of the polarizer settings may produce a mode purity defect up to a few percent [6]. Next, linear coupling of $X$ and $O$ mode waves inevitably occurs in the edge plasma layer, where the anisotropy degenerates. Numerical simulation [9] shows that in this layer an extra power up to 4–6% may be transferred from the $X$ to the $O$ mode. Nonlinear wave effects all along the beam trajectory are also possible sources of anomalous ECRH degradation. As it has been recently claimed [10], a parametric decay of $X$ mode into localized plasma modes may possess a relatively low power threshold and give rise to significant redistribution of wave power deposition. There is also significant experimental evidence supporting the occurrence of such parametric decay instabilities [11,12]. Finally, if the wave vector is almost perpendicular to the magnetic field near the resonance, there exists another linear coupling zone, which approximately coincides with the location of resonant absorption. This effect is unique to second harmonic ECRH and arises due to an extreme surge of the $X$ mode refractive index near the resonance. It has been known for decades [1], but didn't attract a deeper interest. Here we explore the possible impact of such mode coupling on ECRH efficiency by extending the proven asymptotic technique based on the short-wavelength paraxial approximation to the case of two interacting modes in a

[*]maxt@inbox.ru

 

substantially non-Hermitian plasma. The developed method itself is independent of the specific wave mode properties, which are taken into account later via the dispersion tensor eigendecomposition. In contrast to phase space methods based on variational principles [13] and "quasioptical" methods (see, for example, Ref. [14] and the references cited therein) the described technique does not employ the complicated Weyl symbol calculus, which makes it more intelligible for physicists.

This paper is organized as follows. In Sec. II, we present a thorough eigenmode analysis of Gaussian beam propagation, starting from the familiar case of a single independent mode and then arriving at the case of two coupled modes. In Sec. III, we obtain the analytical expressions for eigenvalues and corresponding eigenvectors of the weakly relativistic plasma dispersion tensor for the case of quasiperpendicular wave propagation. We also numerically demonstrate the appearance of non-Hermitian mode coupling near the second harmonic EC resonance. In Sec. IV, we present the results of a numerical simulation that implements the mathematical model described in the previous sections. Section V contains a summary of our study.

## II. AMPLITUDE EQUATIONS FOR INDEPENDENT AND COUPLED MICROWAVE BEAMS

Suppose a monochromatic microwave beam of frequency $\omega$ propagates in a stationary plasma whose inhomogeneity scale is much larger than the wavelength and somewhat larger than the beam width. Absorption, phase front curvature, and polarization variation of the wave also may occur, with a similar condition on the corresponding spatial scales. For brevity, further we will omit all $\exp(-i\omega t)$ factors from the wave-field expressions and will omit $\omega$ from the argument lists. It is convenient to consider the three-dimensional (3D) wave vector equation in the following generic integral form:

$$\int \mathbf{L}\left(\boldsymbol{\rho}, \frac{\mathbf{r}+\mathbf{r}'}{2}\right)\mathbf{E}(\mathbf{r}')d^3\mathbf{r}' = \mathbf{0}, \tag{1}$$

where the complex vector $\mathbf{E}$ is the microwave electric field, $\mathbf{r}$ is the position vector, and $\boldsymbol{\rho} \equiv \mathbf{r} - \mathbf{r}'$ is the nearby displacement. According to Maxwell's equations, the dispersion $3 \times 3$ matrix kernel $\mathbf{L}$ includes the local part, which becomes the partial differential operator after convolution, and the nonlocal plasma conductivity matrix kernel $\boldsymbol{\sigma}$:

$$\mathbf{L} = \left[\frac{c^2}{\omega^2}\nabla\nabla^{\mathrm{T}} - \left(\frac{c^2}{\omega^2}\nabla^{\mathrm{T}}\nabla + 1\right)\mathbf{I}\right]\delta(\boldsymbol{\rho}) - \frac{4\pi i}{\omega}\boldsymbol{\sigma}\left(\boldsymbol{\rho}, \frac{\mathbf{r}+\mathbf{r}'}{2}\right). \tag{2}$$

Here $c$ is the vacuum speed of light, $\mathbf{I}$ is the identity matrix, $\delta(\cdot)$ is the delta function, $T$ denotes the matrix transpose, and to clarify, a vector is a column matrix and, therefore, $\nabla\nabla^{\mathrm{T}}$ is a matrix operator and $\nabla^{\mathrm{T}}\nabla = \nabla \cdot \nabla$ is a scalar operator. Both $\mathbf{L}$ and $\boldsymbol{\sigma}$ depend on their first argument due to spatial dispersion and on the second one due to plasma inhomogeneity. However, the specific form of $\mathbf{L}$ is of no importance for further consideration in this section.

The crucial point in the following asymptotic analysis is the representation of the possibly irregular (noneikonal) wave-field $\mathbf{E}(\mathbf{r})$ as a continuous superposition of locally plane waves,

$$\mathbf{E}(\mathbf{r}) = (2\pi)^{-3}\int \exp(i\mathbf{k}\cdot\mathbf{r})\mathbf{A}(\mathbf{k}, \mathbf{r})d^3\mathbf{k}, \tag{3}$$

which differs from the usual plane wave decomposition (i.e., inverse Fourier transform) in that the amplitudes $\mathbf{A}(\mathbf{k}, \mathbf{r})$ retain all the wave-field spatial inhomogeneity except only the smallest-scale one [resulting from the fast phase variation of $\mathbf{E}(\mathbf{r})$]. This can be done most conveniently [15] using the smoothly windowed local Fourier transform,

$$\mathbf{A}(\mathbf{k}, \mathbf{r}) = \int \exp(-i\mathbf{k}\cdot\mathbf{r}' - |\boldsymbol{\rho}|^2/w^2)\mathbf{E}(\mathbf{r}')d^3\mathbf{r}', \tag{4}$$

with $w$ chosen intermediate between the length scales $|\nabla \ln \tilde{E}|^{-1}$ and $|\nabla \ln \tilde{A}|^{-1}$ (here the tilde denotes the scalar counterpart of the complex vector, i.e., the complex function whose argument is a weighted average of the vector component arguments). The assumption of weak inhomogeneity specifically means that $|\nabla \ln \tilde{A}| \ll |\nabla \ln \tilde{E}|$, hence the definition of Eq. (4) is feasible and it ensures that $\mathbf{A}(\mathbf{k}, \mathbf{r})$ is always a slowly varying function of $\mathbf{r}$, even at caustics [16]. A widely spread 1D prototype of what we do is the representation of a temporal variation in sound intensity as an audio-frequency spectrum that also varies in time, but not very rapidly. The framework of Eqs. (3) and (4) is more general and methodically simple than the WKB method, which picks out only one Fourier component even though admitting that the selected $\mathbf{k}$ may slowly vary in space. In fact, both methods are related as follows. In the case that $\mathbf{E}(\mathbf{r})$ is locally a regular wave field, $\mathbf{A}(\mathbf{k}, \mathbf{r})$ is nonzero only in the close vicinity of $\mathbf{k} = \nabla \arg(\tilde{E})$:

$$\begin{aligned}\mathbf{A}(\mathbf{k}, \mathbf{r}) &\approx \pi^{3/2}w^3\mathbf{E}(\mathbf{r})\exp\left(-i\mathbf{k}\cdot\mathbf{r} - \frac{w^2}{4}|\mathbf{k} - \nabla\arg(\tilde{E})|^2\right)\\ &\to (2\pi)^3\mathbf{E}(\mathbf{r})\exp(-i\mathbf{k}\cdot\mathbf{r})\\ &\quad\times\ \delta[|\mathbf{k} - \nabla\arg(\tilde{E})|] \quad \text{as } w \to \infty.\end{aligned} \tag{5}$$

This expression also demonstrates conformity between the dependencies of $|\mathbf{A}|$ and $|\mathbf{E}|$ on $\mathbf{r}$ away from caustics or other zones where the $\mathbf{k}$ spectrum is not condensed. Seeking $\mathbf{A}(\mathbf{k}, \mathbf{r})$ instead of $\mathbf{E}(\mathbf{r})$ means doubling the problem dimensionality ($\mathbf{k}$ is an independent real vector variable, not a function of $\mathbf{r}$) for the sake of reliability of the asymptotic technique. The reverse projection of $\mathbf{A}$ onto 3D $\mathbf{r}$ space in a specified region is the ultimate goal.

The slow spatial variation of plasma parameters allows one to use the following approximation in Eq. (1):

$$\mathbf{L}\left(\boldsymbol{\rho}, \frac{\mathbf{r}+\mathbf{r}'}{2}\right) \approx \left(1 - \frac{\boldsymbol{\rho}}{2}\cdot\nabla\right)\mathbf{L}(\boldsymbol{\rho}, \mathbf{r}), \tag{6}$$

for displacements within the radius (small compared to $w$) of spatial dispersion. The slow spatial variation of $\mathbf{A}(\mathbf{k}, \mathbf{r})$ justifies the approximation

$$\begin{aligned}\mathbf{E}(\mathbf{r}') \approx (2\pi)^{-3}&\int \exp(i\mathbf{k}\cdot\mathbf{r}')\\ &\times\left(\mathbf{A} - \rho_\alpha\frac{\partial\mathbf{A}}{\partial r_\alpha} + \frac{\rho_\alpha\rho_\beta}{2}\frac{\partial^2\mathbf{A}}{\partial r_\alpha\partial r_\beta}\right)d^3\mathbf{k},\end{aligned} \tag{7}$$

which arises from Eq. (3). From now on, we imply the summation from 1 to 3 over the repeated Greek indices and assume that the coordinates are Cartesian.

It is known [17] that Gaussian beams are the simplest and the most frequent type of microwave beams in laboratory plasmas. In any case, a microwave beam of arbitrary form can be decomposed into a sum of Gaussian beamlets [18]. So to proceed further, we suppose that if $\mathbf{r}$ is a point on the beam axis, then $\partial^2\mathbf{A}/\partial r_\alpha \partial r_\beta \approx i\mathbf{A}Q_{\alpha\beta}$, where the symmetric complex matrix $\mathbf{Q}(\mathbf{r}) \equiv \nabla\nabla^{\mathrm{T}} \arg(\tilde{E})$ is approximately equal to $\nabla\nabla^{\mathrm{T}} \arg(\tilde{A})$ according to Eq. (5). One should note that, for the Gaussian beam wave field $\mathbf{E}(\mathbf{r}')$, six independent entries of Re$\mathbf{Q}$ specifies three parameters of the phase front curvature at $\mathbf{r}$ and six entries of Im$\mathbf{Q}$ specifies another three parameters of the amplitude envelope across the axis. Therefore, both half of Re$\mathbf{Q}$ and half of Im$\mathbf{Q}$ may seem undefined or insignificant, but, as explicated below, they are also strictly determined because $\mathbf{Q}$ is subjected to a certain geometry constraint.

The approximations of Eqs. (6) and (7) imply that all the terms within parentheses which contain spatial derivatives are relatively small. Substitution of Eqs. (6) and (7) into Eq. (1) leads to an equation of the form $\int \exp(i\mathbf{k}\cdot\mathbf{r})\Sigma(\mathbf{k},\mathbf{r})d^3\mathbf{k} = \mathbf{0}$, which requires $\Sigma = \mathbf{0}$. The non-negligible terms from the latter equation constitute the following equation for the slow spatial variation of $\mathbf{A}$ (see Appendix A for details):

$$\mathbf{\Lambda A} - \frac{i}{2}\frac{\partial^2\mathbf{\Lambda}}{\partial k_\alpha \partial r_\alpha}\mathbf{A} - i\frac{\partial\mathbf{\Lambda}}{\partial k_\alpha}\frac{\partial\mathbf{A}}{\partial r_\alpha} - \frac{i}{2}\frac{\partial^2\mathbf{\Lambda}}{\partial k_\alpha \partial k_\beta}\mathbf{A}Q_{\alpha\beta} = \mathbf{0}. \quad (8)$$

Here $\mathbf{\Lambda}(\mathbf{k},\mathbf{r}) \equiv \int \exp(-i\mathbf{k}\cdot\boldsymbol{\rho})\mathbf{L}(\boldsymbol{\rho},\mathbf{r})d^3\boldsymbol{\rho}$ is the local dispersion tensor, which can be expressed through the plasma dielectric tensor $\boldsymbol{\varepsilon}(\mathbf{k},\mathbf{r})$ as $\mathbf{\Lambda} = N^2\mathbf{I} - \mathbf{NN}^{\mathrm{T}} - \boldsymbol{\varepsilon}$, where $\mathbf{N} \equiv \mathbf{k}c/\omega$.

The next step of the analysis is to perform the polarization eigenmode decomposition of Eq. (8). Let us define the matrices $\mathbf{D} \equiv \mathrm{diag}(\lambda^{(1)}, \lambda^{(2)}, \lambda^{(3)})$ and $\mathbf{X} \equiv (\mathbf{x}^{(1)} \quad \mathbf{x}^{(2)} \quad \mathbf{x}^{(3)})$, where the diagonal entries $\lambda^{(m)}$ are the eigenvalues of $\mathbf{\Lambda}$ and the columns $\mathbf{x}^{(m)}$ are the corresponding right eigenvectors such that $|\mathbf{x}^{(m)}| = 1$ while $\arg(\tilde{x}^{(m)})$ are arbitrary. Therefore, $\mathbf{\Lambda X} = \mathbf{XD}$ and, accordingly, $\mathbf{\Lambda} = \mathbf{XDX}^{-1}$. One should point out that while $\mathbf{X}^{-1} = (\mathbf{y}^{(1)} \quad \mathbf{y}^{(2)} \quad \mathbf{y}^{(3)})^{\mathrm{T}}$, where $\mathbf{y}^{(m)}$ are the left eigenvectors obeying $\mathbf{y}^{(m)}\cdot\mathbf{x}^{(n)} = I_{mn}$, this does not always imply $|\mathbf{y}^{(m)}| = 1$ (but if $\mathbf{\Lambda}$ is Hermitian, i.e., $\mathbf{\Lambda} = \mathbf{\Lambda}^{*\mathrm{T}}$, then $\mathbf{y}^{(m)} = \mathbf{x}^{(m)*}$). The notation $U_\alpha^{(mn)} \equiv \mathbf{y}^{(m)}\cdot\partial\mathbf{x}^{(n)}/\partial k_\alpha$ and $V_\alpha^{(mn)} \equiv \mathbf{y}^{(m)}\cdot\partial\mathbf{x}^{(n)}/\partial r_\alpha$ will be used below. We also introduce the vector $\mathbf{z}(\mathbf{k},\mathbf{r}) \equiv \mathbf{X}^{-1}\mathbf{A}$; it is easily seen that $\mathbf{A} = z_\alpha\mathbf{x}^{(\alpha)}$ and so the components of $\mathbf{z}$ are the coefficients of the eigenmode decomposition. Additionally, we will initially use the following matrix notation:

$$\begin{aligned}
\mathbf{G}_\alpha &\equiv \mathbf{X}^{-1}\frac{\partial\mathbf{\Lambda}}{\partial k_\alpha}\mathbf{X},\\
\hat{\mathbf{G}}_{\alpha\beta} &\equiv \mathbf{X}^{-1}\frac{\partial^2\mathbf{\Lambda}}{\partial k_\alpha \partial k_\beta}\mathbf{X},\\
\mathbf{F} &\equiv \mathbf{X}^{-1}\frac{\partial\mathbf{\Lambda}}{\partial k_\alpha}\frac{\partial\mathbf{X}}{\partial r_\alpha} - \frac{\partial\mathbf{X}^{-1}}{\partial r_\alpha}\frac{\partial\mathbf{\Lambda}}{\partial k_\alpha}\mathbf{X},
\end{aligned} \quad (9)$$

some components of which will be expressed later in terms of $\lambda^{(m)}$, $U_\alpha^{(mn)}$, and $V_\alpha^{(mn)}$ (complete expressions are given in Appendix B). Multiplying Eq. (8) with $\mathbf{X}^{-1}$ from the left yields

$$2\mathbf{G}_\alpha\frac{\partial\mathbf{z}}{\partial r_\alpha} + \left(2i\mathbf{D} + \frac{\partial\mathbf{G}_\alpha}{\partial r_\alpha} + \mathbf{F} + \hat{\mathbf{G}}_{\alpha\beta}Q_{\alpha\beta}\right)\mathbf{z} = \mathbf{0}. \quad (10)$$

### A. Independent microwave beam

In the simplest case of a plane wave in a homogeneous plasma one has $\mathbf{F} = \mathbf{0}$, $\mathbf{Q} = \mathbf{0}$, $\partial\mathbf{z}/\partial r_\alpha = \mathbf{0}$, $\partial\mathbf{G}_\alpha/\partial r_\alpha = \mathbf{0}$, and Im$\mathbf{D} = \mathbf{0}$, so Eq. (10) reduces to $\mathbf{Dz} = \mathbf{0}$. The latter expression consists of three independent scalar equations $\lambda^{(m)}z_m = 0$ (without summation over $m$). Evidently, propagation of any particular wave mode is possible only if the corresponding dispersion relation $\lambda^{(m)}(\mathbf{k}) = 0$ is fulfilled. Of course, this case has little to do with microwave behavior in fusion plasmas and it serves just to illustrate how the concept of wave modes emerges from Eq. (10).

In an inhomogeneous plasma all the terms entering Eq. (10) are nonzero, making Eq. (10) consist of three coupled scalar equations. In each of these equations the term $2i\lambda^{(m)}z_m$, which is not *a priori* small, is balanced by the terms containing spatial derivatives, so in a weakly inhomogeneous plasma, the condition $|\lambda^{(m)}| \to 0$ is still necessary for the particular mode to be active. Suppose now that any two functions $|\lambda^{(m)}|$ corresponding to different eigenmodes do not vanish simultaneously at any point of $(\mathbf{k},\mathbf{r})$. This means that only one mode, say $m = 1$, has the distinctive feature $|\lambda^{(1)}| \to 0$ in a certain subspace of $(\mathbf{k},\mathbf{r})$ and, therefore, it alone ($|z_1| \gg |z_2|, |z_3|$) can propagate along some path belonging to this subspace. In other words, this mode is well separated in either $\mathbf{r}$ or $\mathbf{k}$ from the other modes and it can be regarded as independent. It is helpful to write out (see Appendix B for details)

$$\left(\mathbf{G}_\alpha\frac{\partial\mathbf{z}}{\partial r_\alpha}\right)_1 = \frac{\partial\lambda^{(1)}}{\partial k_\alpha}\frac{\partial z_1}{\partial r_\alpha} + \sum_{n\neq 1}(\lambda^{(n)} - \lambda^{(1)})U_\alpha^{(1n)}\frac{\partial z_n}{\partial r_\alpha} \quad (11)$$

and notice that the terms containing $\lambda^{(n)}\partial z_n/\partial\mathbf{r}$ are much less than $|\lambda^{(n)}z_n|$ for all $n$. Only the first term on the right-hand side of Eq. (11) should therefore be retained. Having multiplied the first scalar equation of Eq. (10) by $z_1^*$, we obtain

$$\begin{aligned}
&\frac{\partial}{\partial r_\alpha}\left(\frac{\partial\lambda^{(1)}}{\partial k_\alpha}|z_1|^2\right) + \left(2i\lambda^{(1)} + 2i\frac{\partial\lambda^{(1)}}{\partial k_\alpha}\frac{\partial\arg(z_1)}{\partial r_\alpha} + F_{11}\right.\\
&\left.\quad + \hat{G}_{\alpha\beta 11}Q_{\alpha\beta}\right)|z_1|^2 = 0.
\end{aligned} \quad (12)$$

It may be seen from Eq. (12) that if $\mathbf{\Lambda}$ is non-Hermitian, there exists a new length scale $\sim|\mathrm{Im}\lambda^{(1)}|^{-1}|\partial\mathrm{Re}\lambda^{(1)}/\partial\mathbf{k}|$ of $|z_1|$ inhomogeneity due to absorption. Recalling the condition for all inhomogeneity length scales to be large enough (that was necessary for the above derivation), we conclude that the smallness of $|\mathrm{Im}\lambda^{(1)}|$ is a more general requirement than the essentially local condition $|\mathrm{Re}\lambda^{(1)}| \to 0$. This means that, for our purposes, all terms containing derivatives of $\mathrm{Im}\lambda^{(1)}$ usually contain an extra smallness compared with those containing derivatives of $\mathrm{Re}\lambda^{(1)}$. Another consequence of the stated restriction is that the non-Hermitian deviation of $\mathbf{y}^{(1)}$ from $\mathbf{x}^{(1)*}$, as well as the nonorthogonality of the right

eigenvectors, is small:

$$|\mathbf{y}^{(1)} - \mathbf{x}^{(1)*}|^2 \approx \sum_{n\neq 1} |\mathbf{x}^{(1)*} \cdot \mathbf{x}^{(n)}|^2 \leqslant 4|\mathrm{Im}\lambda^{(1)}| \sum_{n\neq 1} \frac{|\mathrm{Im}\lambda^{(n)}|}{|\lambda^{(1)} - \lambda^{(n)*}|^2} \ll 1 \quad (13)$$

(see, e.g., Ref. [19] for the proof of the left inequality). After omitting the terms, which are thus found to be negligible, from Eq. (12) and splitting the latter into the real and imaginary parts, we have

$$\frac{\partial}{\partial r_\alpha}\left(\frac{\partial \mathrm{Re}\lambda^{(1)}}{\partial k_\alpha}|z_1|^2\right) = \left(2\mathrm{Im}\lambda^{(1)} - \frac{\partial^2 \mathrm{Re}\lambda^{(1)}}{\partial k_\alpha \partial k_\beta}\mathrm{Re}Q_{\alpha\beta} - \mathrm{Re}\chi^{(11)}\right)|z_1|^2, \quad (14)$$

$$\mathrm{Re}\lambda^{(1)} + \frac{\partial \mathrm{Re}\lambda^{(1)}}{\partial k_\alpha}\kappa_\alpha^{(1)} + \frac{1}{2}\frac{\partial^2 \mathrm{Re}\lambda^{(1)}}{\partial k_\alpha \partial k_\beta}\mathrm{Im}Q_{\alpha\beta} + \frac{1}{2}\mathrm{Im}\chi^{(11)} = 0, \quad (15)$$

where $\boldsymbol{\kappa}^{(1)} \equiv \nabla \arg(z_1) + |x_\alpha^{(1)}|^2 \nabla \arg(x_\alpha^{(1)})$ and $\chi^{(11)} \equiv \sum_{n\neq 1} \lambda^{(n)}[U_\alpha^{(1n)}V_\alpha^{(n1)} - U_\alpha^{(n1)}V_\alpha^{(1n)} - 2U_\alpha^{(1n)}Q_{\alpha\beta}U_\beta^{(n1)}]$. It is worth noting that $\boldsymbol{\kappa}^{(1)}$ and $\chi^{(11)}$ are both invariant under the changes $\mathbf{x}^{(m)} \to \mathbf{x}^{(m)}\exp(i\varphi^{(m)})$ with arbitrary real $\varphi^{(m)}$ provided that $\arg(z_1\tilde{x}^{(1)})$ is unchanged.

A physical interpretation of Eqs. (14) and (15) directly comes from their mathematical properties. The continuity Eq. (14) is definitely a wave power transport equation and it reveals that the wave power flux, which is proportional to the vector under the divergence operator on the left-hand side, is collinear with $\partial \mathrm{Re}\lambda^{(1)}/\partial \mathbf{k}$. Equation (15) is algebraic and does not contain $|z_1|$. It is a condition of radiative transparency, i.e., a modified dispersion relation, which does not merely impose a constraint on $\mathbf{k}$ by the terms dependent only on $\mathbf{k}$ and $\mathbf{r}$, but also specifies the gradient of an additional phase shift $\arg(z_1\tilde{x}^{(1)})$ due to the nonzero $\mathbf{Q}$. This phase shift contains, for example, the Gouy phase shift [17,20], which arises due to the third term in Eq. (15) and evolves slowly everywhere except near the microwave beam waists. All the terms of Eq. (15) are small compared to 1, therefore similarly one can consider Eq. (15) with $\mathrm{Re}\lambda^{(1)}(\mathbf{k},\mathbf{r}) = 0$ being the main condition and $\nabla \arg(z_1\tilde{x}^{(1)})$ being the compensation for the remaining terms. In this way, Eqs. (14) and (15) give an alternative reasoning (compared to the standard WKB approach [21,22]) of why and how the short-wavelength paraxial asymptotic technique should involve the numerical algorithm known as "ray tracing." This algorithm consists in calculating, starting from given initial values, two parametrically defined 3D curves $\mathbf{R}(s)$ and $\mathbf{K}(s)$, which are respectively the spatial trajectory of wave power transport (and hence may be the axis of a propagating Gaussian beam) and the corresponding evolution of $\mathbf{k}$ that continuously satisfies the dispersion relation. Up to a constant factor, Eq. (14) yields $d\mathbf{R}/ds = \partial \mathrm{Re}\lambda^{(1)}/\partial \mathbf{k}$, which, taken together with the condition $\mathrm{Re}\lambda^{(1)}(\mathbf{K},\mathbf{R}) = 0$, requires $d\mathbf{K}/ds = -\partial \mathrm{Re}\lambda^{(1)}/\partial \mathbf{r}$; the derivatives should be estimated at $\mathbf{r} = \mathbf{R}(s)$ and $\mathbf{k} = \mathbf{K}(s) + \nabla \arg(z_1\tilde{x}^{(1)})$. The vector $d\mathbf{R}/ds$ is thus proportional to the group velocity $\mathbf{v}_\mathrm{g} \equiv -(\partial \mathrm{Re}\lambda^{(1)}/\partial \mathbf{k})(\partial \mathrm{Re}\lambda^{(1)}/\partial \omega)^{-1}$, which gives the proper sign for the increments of $s$ in the calculation. Within the "beam tracing" framework [23,24], the matrix $\mathbf{Q}$ is also a function of $s$. The equation for $d\mathbf{Q}/ds$, which is not required herein, is nothing but a conservation condition for the universal geometry constraint $\mathbf{Q}d\mathbf{R}/ds = d\mathbf{K}/ds$ along an arbitrary path $\mathbf{R}(s)$ (see Ref. [25] for the details).

In the regular propagation regime, it follows from Eq. (5) that the magnitudes of the wave field at the beam axis $\mathbf{E}_R(s) = \mathbf{E}(\mathbf{R})$ and the value $z_1(\mathbf{k},\mathbf{R})$ are related as $|z_1| = |\mathbf{E}_R g(\mathbf{k})|$, where $g(\mathbf{k})$ is a narrow Gaussian function, so that one can write

$$\frac{d|\mathbf{E}_R|^2}{ds} = |g|^{-2}\frac{d\mathbf{R}}{ds}\cdot\nabla|z_1|^2 = |g|^{-2}\frac{\partial}{\partial r_\alpha}\left(\frac{\partial \mathrm{Re}\lambda^{(1)}}{\partial k_\alpha}|z_1|^2\right) - \frac{\partial^2 \mathrm{Re}\lambda^{(1)}}{\partial r_\alpha \partial k_\alpha}|\mathbf{E}_R|^2. \quad (16)$$

Equations (14) and (16) combine into the equation

$$\frac{d}{ds}\ln|\mathbf{E}_R|^2 = 2\mathrm{Im}\lambda^{(1)} - \frac{\partial^2 \mathrm{Re}\lambda^{(1)}}{\partial r_\alpha \partial k_\alpha} - \frac{\partial^2 \mathrm{Re}\lambda^{(1)}}{\partial k_\alpha \partial k_\beta}\mathrm{Re}Q_{\alpha\beta} - \mathrm{Re}\chi^{(11)}. \quad (17)$$

Gaussian beams possess the following feature, which is conserved during propagation: one of the eigenvalues of $\mathrm{Im}\mathbf{Q}$ is zero and the other two (say, $\tau_1$ and $\tau_2$) are positive. It was shown in Ref. [25] that one can present Eq. (17) in a more physically intelligible form that reveals the eigenmode power balance:

$$\frac{d}{ds}\ln\left(|\mathbf{E}_R|^2 S\left|\frac{d\mathbf{R}}{ds}\right|\right) = 2\mathrm{Im}\lambda^{(1)} - \mathrm{Re}\chi^{(11)}, \quad (18)$$

where $S \equiv (\tau_1\tau_2)^{-1/2}$ is, up to a factor, the beam cross area. The first term on the right-hand side of Eq. (18) accounts for the actual power dissipation. The last term, which is usually negligible, is responsible for practically small "artificial" deviations in power, which may arise since our definition of eigenmodes comes from simple diagonalization of $\boldsymbol{\Lambda}$ rather than from cumbersome diagonalization of Eq. (8) (see, for example, Ref. [26]).

### B. Coupled microwave beams

Now let us consider the case of two modes being active together within some zone of $(\mathbf{k},\mathbf{r})$ (hereafter the bizone, BZ), where $|\lambda^{(1)}|, |\lambda^{(2)}| \to 0$. Equation (10) was obtained under the paraxial assumption, which implies that only one spatial axis exists. Two different active modes generally propagate in plasmas as two beams whose ray trajectories $\mathbf{R}^{(m)}(s)$ and $\mathbf{K}^{(m)}(s)$ $(m = 1, 2)$ cross (or nearly cross) within the BZ, but may not be parallel. However, we will suppose below that both $d\mathbf{R}^{(m)}/ds$ are collinear in the BZ, so the paraxial approximation (7) is justified, and hence Eq. (10) is valid. It was demonstrated in Ref. [27] that any two beams can be brought into coaxiality within the BZ by changing over to a specially oriented hybrid $(k_1 \quad r_2 \quad r_3)^\mathrm{T}$ representation, in which a similar paraxial formalism may be developed. Therefore, the subsequent analysis can also be adapted to immediately bifurcating beams.

We allow for the beams to possess different $\mathbf{Q}^{(m)}(s)$. This means that one has to replace $Q_{\alpha\beta}z_m$ in Eq. (10) with $Q_{\alpha\beta}^{(m)}z_m$.

Having multiplied the first two equations of Eq. (10) respectively by $z_1^*$ and $z_2^*$, we obtain two equations of the same form,

$$\frac{\partial}{\partial r_\alpha}\left(\frac{\partial\lambda^{(m)}}{\partial k_\alpha}|z_m|^2\right)+\left(2i\lambda^{(m)}+2i\frac{\partial\lambda^{(m)}}{\partial k_\alpha}\frac{\partial\arg(z_m)}{\partial r_\alpha}+F_{mm}+\hat{G}_{\alpha\beta mm}Q^{(m)}_{\alpha\beta}\right)|z_m|^2+\left(F_{m\bar m}+\hat{G}_{\alpha\beta m\bar m}Q^{(\bar m)}_{\alpha\beta}\right)z_m^*z_{\bar m}=0, \tag{19}$$

where the pair $(m,\bar m)$ is either (1, 2) or (2, 1). In the case of nearly degenerate eigenvalues, the corresponding eigenvectors are not guaranteed to be almost orthogonal, which is seen since the right inequality of Eq. (13) is not valid in the BZ. Nevertheless, any linear combination of such eigenvectors is also an eigenvector and hence one can redefine $\mathbf{x}^{(m)}$ via Gram-Schmidt orthogonalization such that the deviation of $\mathbf{y}^{(m)}$ from $\mathbf{x}^{(m)*}$ remains small. Thus in the same way as above, Eq. (19) yields the following power transport equation and the modified dispersion relation for either of the active modes 1 and 2:

$$\frac{\partial}{\partial r_\alpha}\left(\frac{\partial\mathrm{Re}\lambda^{(m)}}{\partial k_\alpha}|z_m|^2\right)=\left(2\mathrm{Im}\lambda^{(m)}-\frac{\partial^2\mathrm{Re}\lambda^{(m)}}{\partial k_\alpha\partial k_\beta}\mathrm{Re}Q^{(m)}_{\alpha\beta}-\mathrm{Re}\chi^{(mm)}\right)|z_m|^2-\mathrm{Re}(\eta^{(m)}z_m^*z_{\bar m}), \tag{20}$$

$$\mathrm{Re}\lambda^{(m)}+\frac{\partial\mathrm{Re}\lambda^{(m)}}{\partial k_\alpha}\kappa^{(m)}_\alpha+\frac{1}{2}\frac{\partial^2\mathrm{Re}\lambda^{(m)}}{\partial k_\alpha\partial k_\beta}\mathrm{Im}Q^{(m)}_{\alpha\beta}+\frac{1}{2}\mathrm{Im}\left(\chi^{(mm)}+\eta^{(m)}\frac{z_{\bar m}}{z_m}\right)=0, \tag{21}$$

where $\boldsymbol{\kappa}^{(m)}\equiv\nabla\arg(z_m)+|x^{(m)}_\alpha|^2\nabla\arg(x^{(m)}_\alpha)$, $\chi^{(mn)}\approx\lambda^{(3)}[U^{(m3)}_\alpha V^{(3n)}_\alpha-U^{(3n)}_\alpha V^{(m3)}_\alpha-2U^{(m3)}_\alpha Q^{(n)}_{\alpha\beta}U^{(3n)}_\beta]$,

$$\eta^{(m)}\equiv\frac{\partial(\lambda^{(m)}+\lambda^{(\bar m)})}{\partial k_\alpha}V^{(m\bar m)}_\alpha+2\frac{\partial(\lambda^{(\bar m)}-\lambda^{(m)})}{\partial k_\alpha}Q^{(\bar m)}_{\alpha\beta}U^{(m\bar m)}_\beta+\chi^{(m\bar m)}. \tag{22}$$

One can see from Eq. (21) that the phase coherence condition $\mathrm{Im}(\eta^{(m)}z_{\bar m}/z_m)=0$ must be fulfilled so the two active modes remain close in $\mathbf{k}$ space for a while. In particular, it defines the initial phase of the "newborn" mode driven by the "parent" beam in the BZ.

In order to obtain the coupled beam axis amplitude equations for the regular propagation regime, we have to define $d\mathbf{R}^{(m)}/ds=\gamma^{(m)}\partial\mathrm{Re}\lambda^{(m)}/\partial\mathbf{k}$ and choose the calibrating constant factors $\gamma^{(m)}$ such that $d\mathbf{R}^{(1)}/ds=d\mathbf{R}^{(2)}/ds$ in the BZ (hence one can omit the superscript from $\mathbf{R}$), because both of the values $\mathbf{E}^{(m)}_R(s)$ must correspond to the same position. Of course this necessitates the definition $d\mathbf{K}^{(m)}/ds=-\gamma^{(m)}\partial\mathrm{Re}\lambda^{(m)}\partial\mathbf{r}$. Now let $z_m=\tilde E^{(m)}_R g(\mathbf{k})\exp(-i\mathbf{k}\cdot\mathbf{R})$, where $\tilde E^{(m)}_R=\mathbf{x}^{(m)*}\cdot\mathbf{E}^{(m)}_R$, since both of the modes share the same Gaussian $g(\mathbf{k})$ in the BZ. This is justified by the fact that the discrepancy $|\mathbf{K}^{(2)}-\mathbf{K}^{(1)}|$ within the BZ has an upper estimate of $\sim\Delta R^{-1}\ll w^{-1}$, where $\Delta R$ is the BZ length. As a consequence,

$$\frac{d\left|\mathbf{E}^{(m)}_R\right|^2}{\gamma^{(m)}ds}=|g|^{-2}\frac{\partial}{\partial r_\alpha}\left(\frac{\partial\mathrm{Re}\lambda^{(m)}}{\partial k_\alpha}|z_m|^2\right)-\frac{\partial^2\mathrm{Re}\lambda^{(m)}}{\partial r_\alpha\partial k_\alpha}\left|\mathbf{E}^{(m)}_R\right|^2,$$

$$z_m^*z_{\bar m}=\tilde E^{(m)*}_R\tilde E^{(\bar m)}_R|g|^2, \tag{23}$$

which, together with Eq. (20), results in the amplitude equation

$$2\frac{d\left|\mathbf{E}^{(m)}_R\right|}{\gamma^{(m)}ds}=\left(2\mathrm{Im}\lambda^{(m)}-\frac{\partial^2\mathrm{Re}\lambda^{(m)}}{\partial r_\alpha\partial k_\alpha}-\frac{\partial^2\mathrm{Re}\lambda^{(m)}}{\partial k_\alpha\partial k_\beta}\mathrm{Re}Q^{(m)}_{\alpha\beta}-\mathrm{Re}\chi^{(mm)}\right)\left|\mathbf{E}^{(m)}_R\right|-(W^{(m)}_-+W^{(m)}_+)\left|\mathbf{E}^{(\bar m)}_R\right|, \tag{24}$$

where

$$W^{(m)}_\pm\equiv\mathrm{Re}\left[\frac{\eta^{(m)}\pm\eta^{(\bar m)*}}{2}\frac{\tilde E^{(m)*}_R\tilde E^{(\bar m)}_R}{\left|\mathbf{E}^{(m)}_R\right|\left|\mathbf{E}^{(\bar m)}_R\right|}\right].$$

Equation (24) is the main analytical result of this work. Like in the nondissipative case [27], it is of the Budden-Kravtsov type [28,29]. At the same time, it differs from Eq. (17) only in the appearance of the last term. We have split the last term into two parts containing $W^{(m)}_-=-W^{(\bar m)}_-$ and $W^{(m)}_+=W^{(\bar m)}_+$. The former describes the power exchange between the active modes, whereas the latter is mainly a correction accounting for the unequal group velocities of the active modes. In the case that $\mathbf{R}(s)$ and $\mathbf{K}^{(m)}$ are known, the system of differential equations to be solved numerically in the BZ includes three equations: two of the form of Eq. (24) with $m=1$, $\bar m=2$ and vice versa, and the phase difference equation

$$\frac{d}{ds}\left[\arg\left(\tilde E^{(2)}_R\right)-\arg\left(\tilde E^{(1)}_R\right)\right]\approx\frac{d\mathbf{R}}{ds}\cdot(\mathbf{K}^{(2)}-\mathbf{K}^{(1)}). \tag{25}$$

If the mode being born in the BZ is numbered 1, the imposed initial conditions are $|\mathbf{E}^{(1)}_R|=0$, $\mathbf{K}^{(1)}=\mathbf{K}^{(2)}$ and $\arg(\tilde E^{(2)}_R)-\arg(\tilde E^{(1)}_R)=\pi-\arg(\eta^{(1)})$. The latter one combines the phase coherence condition with the requirement $W^{(1)}_-+W^{(1)}_+<0$, which is necessary for $|\mathbf{E}^{(1)}_R|$ to start increasing, according to Eq. (24). The initial value of $\mathrm{Im}\mathbf{Q}^{(1)}$ must be equal to $\mathrm{Im}\mathbf{Q}^{(2)}$ such that the newborn beam inherits the cross section amplitude profile of the parent beam. The initial six independent entries of $\mathrm{Re}\mathbf{Q}^{(1)}$ are found from the following equations: (i) three of the form $\mathbf{v}^{(\alpha)\mathrm{T}}\mathrm{Re}\mathbf{Q}^{(1)}\mathbf{v}^{(\beta)}=\mathbf{v}^{(\alpha)\mathrm{T}}\mathrm{Re}\mathbf{Q}^{(2)}\mathbf{v}^{(\beta)}$ with $\alpha$ and $\beta$ being either 1 or 2, where the real vectors $\mathbf{v}^{(1)}$ and $\mathbf{v}^{(2)}$ are both orthogonal to $\mathbf{K}^{(2)}$ (the conditions for inheritance of the equiphase surface in the paraxial approximation), and (ii) the vector equation $\mathrm{Re}\mathbf{Q}^{(1)}d\mathbf{R}/ds=d\mathbf{K}^{(1)}/ds$ (the geometry constraint).

The two active modes remain coupled along $s$ until their phase difference is $\sim\pi/2$ due to the accumulation described by Eq. (25). After that the values of $\arg(\tilde E^{(1)}_R)$ and $\arg(\tilde E^{(2)}_R)$ start to drift apart more rapidly, which soon results in $z_m^*z_{\bar m}\to 0$, because the peaks of particular Gaussians $g^{(m)}(\mathbf{k})$ do not overlap any more. The BZ condition $|\lambda^{(1)}\pm\lambda^{(2)}|\to 0$ also breaks down and the modes propagate away as independent beams. However, in cases with resonant dissipation the power

transfer between the modes can be terminated even before that, if the parent beam is completely absorbed within the BZ.

## III. EIGENDECOMPOSITION OF THE DISPERSION TENSOR

In the following analysis, we neglect collisional corrections to the dispersion tensor and suppose that the background electron velocity distribution is Maxwellian. Let the axes of local Cartesian coordinates be oriented such that the ambient magnetic field $\mathbf{B} = (0 \quad 0 \quad B)^{\mathrm{T}}$ and $\mathbf{N} = (N_\perp \quad 0 \quad N_{||})^{\mathrm{T}}$; let $m_\mathrm{e}$ be the electron mass and $T_\mathrm{e}$ the electron temperature in energy units. If the frequency of interest $\omega$ is below the third EC harmonic, but is high enough to disregard ion motion, the dispersion tensor obtained within the weakly relativistic approximation $\mu \equiv m_\mathrm{e}c^2/T_\mathrm{e} \gg 1$ (see, e.g., Refs. [1,30–34]) with the extra condition $\mu \gg 4N^2$ takes the form

$$\mathbf{\Lambda} \approx \begin{pmatrix} N_{||}^2 + M_1 & -iM_2 & N_{||}N_\perp(M_4-1) \\ iM_2 & N^2 + M_1 & iN_{||}N_\perp M_4 \\ N_{||}N_\perp(M_4-1) & -iN_{||}N_\perp M_4 & N_\perp^2 + M_3 \end{pmatrix}, \tag{26}$$

where

$$M_1 \equiv -1 + \frac{q\mu}{2}\left(\mathcal{F}_{5/2}^{[-1]} + \mathcal{F}_{5/2}^{[1]} + \frac{N_\perp^2}{u\mu}\mathcal{F}_{7/2}^{[-2]}\right),$$

$$M_2 \equiv \frac{q\mu}{2}\left(\mathcal{F}_{5/2}^{[-1]} - \mathcal{F}_{5/2}^{[1]} + \frac{N_\perp^2}{u\mu}\mathcal{F}_{7/2}^{[-2]}\right),$$

$$M_3 \equiv -1 + q + \frac{qN_\perp^2}{2u}\left(\bar{\mathcal{F}}_{7/2}^{[-1]} + \frac{N_\perp^2}{4u\mu}\bar{\mathcal{F}}_{9/2}^{[-2]}\right),$$

$$M_4 \equiv \frac{q\mu}{2\sqrt{u}}\left[\mathcal{F}_{5/2}^{[-1]} - \mathcal{F}_{7/2}^{[-1]} + \frac{N_\perp^2}{2u\mu}\left(\mathcal{F}_{7/2}^{[-2]} - \mathcal{F}_{9/2}^{[-2]}\right)\right],$$

$$\bar{\mathcal{F}}_\nu^{[l]} \equiv \mathcal{F}_\nu^{[l]} + 2a\left(\mathcal{F}_{\nu-1}^{[l]} - 2\mathcal{F}_\nu^{[l]} + \mathcal{F}_{\nu+1}^{[l]}\right),$$

$$\mathcal{F}_\nu^{[l]} \equiv \mathcal{F}_\nu(\xi_l, a) \equiv -i\int_0^\infty \frac{dt}{(1-it)^\nu}\exp\left(i\xi_l t - \frac{at^2}{1-it}\right),$$

$\xi_l \equiv \mu(1 + l\sqrt{u})$, $a \equiv \mu N_{||}^2/2$, $q \equiv \omega_\mathrm{pe}^2/\omega^2$, $u \equiv \omega_\mathrm{ce}^2/\omega^2$, and $\omega_\mathrm{pe}$ and $\omega_\mathrm{ce}$ are the electron plasma frequency and gyrofrequency. The function $\mathcal{F}_\nu$ is usually referred to as the Shkarofsky function, tracing back to Ref. [30]. For a large argument $|\xi_l| \gg 1$, this function varies as $\mathcal{F}_\nu^{[l]} \approx (\xi_l + \nu)^{-1}$. Hence, far from the EC harmonic resonances, Eq. (26) reduces to the well-known cold plasma limit. If $a \gg 1$, $\mathcal{F}_\nu^{[l]}$ can be approximated through the nonrelativistic plasma dispersion function.

Assuming $N_{||}^2 \ll 1$, from the equation $\det(\mathbf{\Lambda} - \lambda^{(m)}\mathbf{I}) = 0$ we obtain with an accuracy up to $o(N_{||}^2)$

$$\lambda^{(1)} \approx \lambda_0^{(1)} + N_{||}^2 N_\perp^2 \frac{\lambda_0^{(1)}\left(1 - 2M_4 + 2M_4^2\right) - \psi}{\left(\lambda_0^{(1)} - M_1\right)\left(\lambda_0^{(1)} - N_\perp^2 - M_1\right) - M_2^2},$$

$$\lambda^{(\ell)} \approx \lambda_0^{(\ell)} + N_{||}^2 + N_{||}^2 N_\perp^2 \frac{\lambda_0^{(\ell)}\left(1 - 2M_4 + 2M_4^2\right) - \psi}{\left(\lambda_0^{(\ell)} - \lambda_0^{(1)}\right)\left(2\lambda_0^{(\ell)} - N_\perp^2 - 2M_1\right)}, \tag{27}$$

where $\psi \equiv M_1M_4^2 + 2(1-M_4)M_2M_4 + (1-M_4)^2(N_\perp^2 + M_1)$, $\ell$ is either 2 or 3, and

$$\lambda_0^{(1)} = N_\perp^2 + M_3,$$

$$\lambda_0^{(\ell)} = M_1 + N_\perp^2/2 \pm \sqrt{M_2^2 + N_\perp^4/4} \tag{28}$$

are the eigenvalues of $\mathbf{\Lambda}$ at $N_{||} = 0$ (the upper sign corresponds to $\ell = 2$ and the lower to $\ell = 3$). In what follows, we consider only the second harmonic ECRH, that is the case of $|\xi_{-2}| \ll \mu$, because near the first harmonic resonance the nearly perpendicularly propagating modes remain well separated in $\mathbf{k}$ space. The condition $N_\perp^2 \leqslant 0.918$, which is fulfilled near the resonance in practically all ECRH schemes, is sufficient to ensure that $-\pi/2 < \arg(M_2) \leqslant 0$ and, consequently, $-\pi < \arg(M_2^2 + N_\perp^4/4) \leqslant 0$. Hence, from now on we assume that $\sqrt{M_2^2 + N_\perp^4/4}$ denotes the branch whose imaginary part is negative. The plane-wave dispersion relations for $O$ and $X$ modes are $\mathrm{Re}\lambda^{(1)} = 0$ and $\mathrm{Re}\lambda^{(2)} = 0$, respectively. The equation $\mathrm{Re}\lambda^{(3)} = 0$ (the dispersion relation for the slow extraordinary mode gradually evolving into the electron Bernstein mode) has no roots at $q < 1-u$ and $N_\perp^2 \leqslant 1$.

Figure 1 shows the dispersion surfaces $N_\perp^2(q,u)$ obtained by numerical solution of the equations $\mathrm{Re}\lambda^{(1,2)}(N_\perp^2) = 0$ and the distribution of $-\mathrm{Im}\lambda_0^{(2)}$ over $(q,u)$ evaluated at the corresponding dispersion surface. A prominent feature of the $X$ mode dispersion surface is the spikelike deformation located near the resonance ($u = 0.25$), whose extent along $u$ is proportional to $T_\mathrm{e}$ and whose amplitude is maximum at $N_{||} = 0$. As a result, in the range $N_{||}^2 < 5\mu^{-1}$ the dispersion surfaces of $O$ and $X$ mode waves have common points near the resonance at densities that may occur in ECRH experiments. These points correspond to the BZ locations. In order to perceive the dispersion curves of both modes around the resonance in a 1D slab geometry, one has to look, e.g., at the $q = \mathrm{const}$ slices of Figs. 1(b) and 1(c).

The $X$ mode surge of $N_\perp^2$ around the resonance does not appear in the Appleton-Hartree dispersion relation, which corresponds to the $\mu \to \infty$ limit. That is why the effect of linear mode coupling between the $X$ and $O$ mode waves near the second harmonic EC resonance at $N_{||} \to 0$ is not widely known. This effect can result in malfunction of the ray-tracing algorithm (uncontrolled mode jumps and hence incorrect absorption calculations), if no special precautions are taken. However, besides this, the model of independent beams is not valid in the BZ and must be replaced with the model of Sec. II B. The latter model allows one to combine the ray/beam tracing technique with the consideration of cross-mode interactions.

It is evident from Figs. 1(a) and 1(d) that non-Hermitian plasma dispersion is not only of primary importance for this type of mode coupling, but is also the origin of this effect. Indeed, the peak in $\mathrm{Im}\lambda^{(2)}$ near the resonance coincides with the fast variation of $\arg(\lambda^{(2)})$ in the range between $-\pi$ and 0. Therefore, at fixed values of $N_\perp^2$ and $N_{||}^2$, the function $\mathrm{Re}\lambda^{(2)}$ undergoes a distortion of similar amplitude. The spikelike behavior of $N_\perp^2$, required to satisfy the dispersion relation, is the compensation for such a distortion. Of course, the account of non-Hermitian polarization deviations in the values of $V_\alpha^{(mn)}$ and $U_\alpha^{(mn)}$ is obligatory in this case.

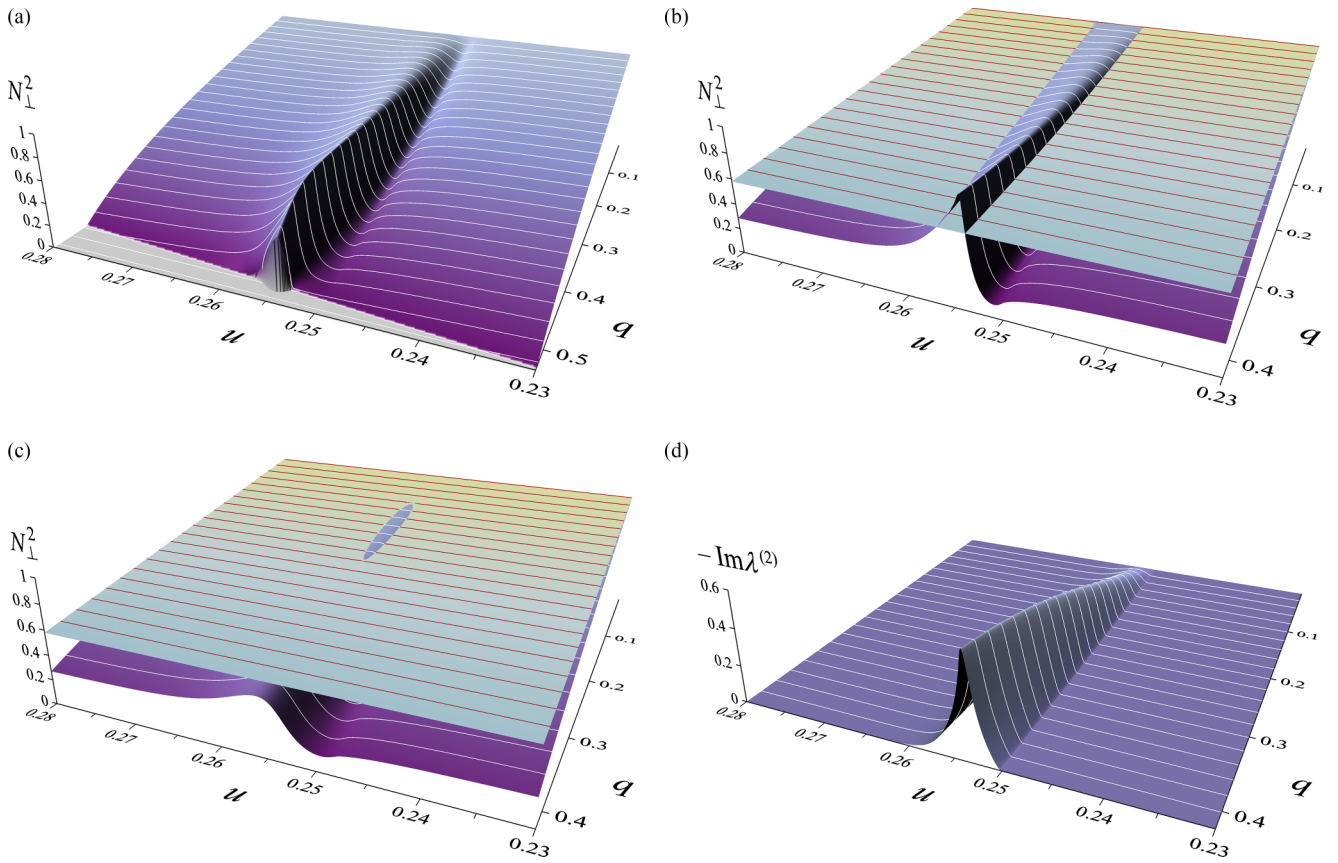


FIG. 1. Vicinity of the second harmonic EC resonance: (a) $X$ mode dispersion surface ($\mathrm{Re}\lambda^{(2)} = 0$) at $N_\parallel^2 = 0$, $\mu = 511$ (i.e., $T_e \approx 1$ keV); (b) part of (a), but with the $O$ mode dispersion surface ($\mathrm{Re}\lambda^{(1)} = 0$) superimposed; (c) the same as (b), but at $N_\parallel^2 = 4.5\mu^{-1}$; (d) distribution of $-\mathrm{Im}\lambda_0^{(2)}$ evaluated at the dispersion surface (a).

Recalling that $(\mathbf{\Lambda} - \lambda^{(m)}\mathbf{I})\mathrm{adj}(\mathbf{\Lambda} - \lambda^{(m)}\mathbf{I}) = \mathbf{0}$, let us select (just to be explicit) the following three vectors from the columns of matrices $\mathrm{adj}(\mathbf{\Lambda} - \lambda^{(m)}\mathbf{I})$ with different $m$:

$$\mathbf{j}^{(1)} = \begin{pmatrix} N_{||}N_\perp[(M_4-1)(\lambda^{(1)} - N^2 - M_1) + M_2M_4] \\ iN_{||}N_\perp[M_4(\lambda^{(1)} - N_{||}^2 - M_1) + M_2(M_4-1)] \\ (\lambda^{(1)} - N_{||}^2 - M_1)(\lambda^{(1)} - N^2 - M_1) - M_2^2 \end{pmatrix},$$

$$\mathbf{j}^{(\ell)} = \begin{pmatrix} (\lambda^{(\ell)} - N^2 - M_1)\left(\lambda^{(\ell)} - \lambda_0^{(1)}\right) - N_{||}^2N_\perp^2M_4^2 \\ iM_2\left(\lambda^{(\ell)} - \lambda_0^{(1)}\right) + iN_{||}^2N_\perp^2M_4(M_4-1) \\ N_{||}N_\perp[(M_4-1)(\lambda^{(\ell)} - N^2 - M_1) + M_2M_4] \end{pmatrix}, \tag{29}$$

where again $\ell$ is either 2 or 3. We may write out the normalized right and the proper left eigenvectors of $\mathbf{\Lambda}$ as $\mathbf{x}^{(m)} = \mathbf{j}^{(m)}|\mathbf{j}^{(m)}|^{-1}$, $\mathbf{y}^{(m)} = \mathbf{j}^{(m')} \times \mathbf{j}^{(m'')}|\mathbf{j}^{(m)}|J^{-1}$, where the triplet $(m, m', m'')$ is one of the permutations $(1, 2, 3)$, $(2, 3, 1)$, $(3, 1, 2)$, and $J \equiv \mathbf{j}^{(m)} \cdot (\mathbf{j}^{(m')} \times \mathbf{j}^{(m'')})$. Accordingly, we have

$$V_\alpha^{(mn)} = \frac{|\mathbf{j}^{(m)}|}{|\mathbf{j}^{(n)}|J} \frac{\partial \mathbf{j}^{(n)}}{\partial r_\alpha} \cdot (\mathbf{j}^{(m')} \times \mathbf{j}^{(m'')}) \tag{30}$$

and a similar (with $r_\alpha$ replaced by $k_\alpha$) expression for $U_\alpha^{(mn)}$. The obtained closed formulas for $\lambda^{(m)}$, $U_\alpha^{(mn)}$, and $V_\alpha^{(mn)}$ allow one to undertake the following numerical analysis.

## IV. X-TO-O MODE POWER TRANSFER IN THE STRICTLY PERPENDICULAR PROPAGATION CASE

In the numerical simulation reported below we restrict our study to the single magnitude $N_{||} = 0$. In this case both vectors $d\mathbf{R}^{(m)}/ds \propto \mathbf{K}^{(m)}\partial\mathrm{Re}\lambda^{(m)}/\partial N_\perp$ ($m = 1, 2$) are collinear in the BZ and can be equated, and so the results of Sec. II B can be directly applied. Although slightly nonperpendicular wave propagation is of methodical importance, in practice one can expect only small deviations from the strictly perpendicular propagation case. Let us orient the axes such that $\mathbf{K}^{(m)} = (K \quad 0 \quad 0)^{\mathrm{T}}$ and $\mathbf{B} = (0 \quad 0 \quad B)^{\mathrm{T}}$ in the BZ. Then the $2 \times 2$ submatrices of $\mathbf{Q}^{(m)}$ alone, formed by deleting the first rows and first columns, characterize the equiphase surfaces and the cross section amplitude profiles of the beams. The other entries must be equal to $\mathbf{Q}_{1\alpha}^{(m)} = |d\mathbf{R}/ds|^{-1}dK_\alpha^{(m)}/ds$.

We explicitly suppose here that the microwave radiation comes to the BZ as a regularly propagating Gaussian beam. This may seem merely a convenient demonstration of the procedure described in Sec. II B, but in fact, considering Gaussian beams is enough to determine whether the non-Hermitian mode coupling effect can be a disturbance for ECRH. One can imagine two questionable situations: (i) The wave field forms a fold caustic in the resonance region if the plasma density approaches the $X$ mode cutoff value $q \approx 1 - \sqrt{u}$ [it is almost the same as in a cold plasma, cf. Fig. 1(a)]. In such a case, the second harmonic ECRH efficiency drastically falls down

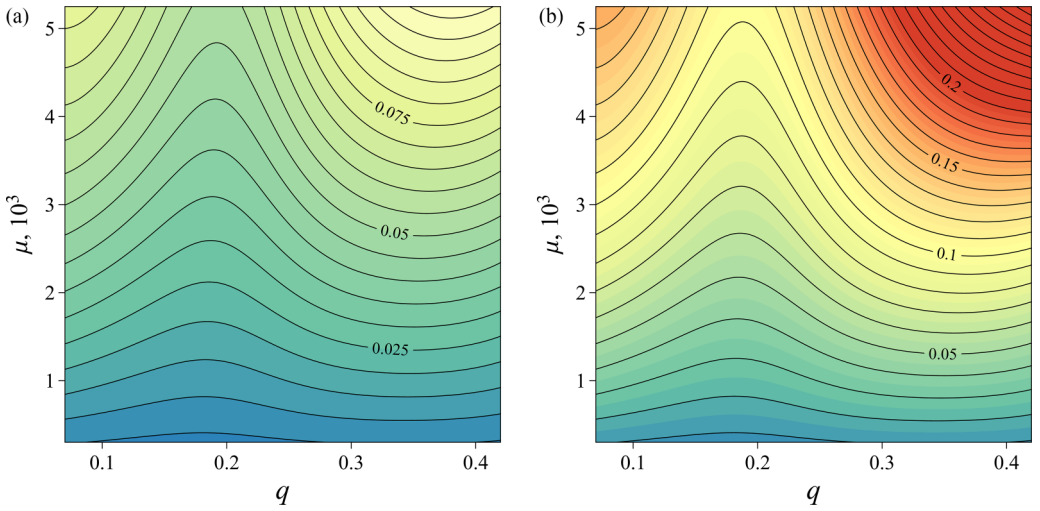


FIG. 2. Relative amplitude of the $O$ mode generated in the BZ by the $X$ mode beam with $N_{||} = 0$, when the magnitude of $\Gamma$ is equal to (a) $10^{-4}$, (b) $2 \times 10^{-4}$.

and so there is no practical reason to study the importance of mode coupling. Moreover, in the vicinity of the cutoff the mode coupling merely disappears. (ii) The microwave beam comes to the resonance layer at a rather oblique angle such that strong variation in plasma dispersion properties across the beam violates the paraxial approximation. In this case, the following computational workaround exists [18]: At the equiphase surface selected right before the resonance layer, a 2D discrete Gabor expansion of the wave field is performed. The results provide the initial amplitudes for a nearly equivalent set (several hundred) of distributed narrower Gaussian beamlets, which then can be traced forward independently (and summed up into a whole wave field, if necessary). Each beamlet thus satisfies the paraxial approximation, while the outcome of this section is also applicable to all of them.

In the typical layout of second harmonic ECRH, the magnetic field inhomogeneity contribution to $\nabla \mathbf{j}^{(n)}$ in the BZ overrides all other contributions due to $\mu \gg 1$, such that in Eq. (30)

$$\frac{\partial \mathbf{j}^{(n)}}{\partial r_\alpha} \approx -2\mu\sqrt{u}\frac{\partial B}{B\partial r_\alpha}\frac{\partial \mathbf{j}^{(n)}}{\partial \xi_{-2}}.$$

Therefore, we will disregard changes of electron density and temperature as well as the magnetic shear within the BZ in the simulations. A brief examination of Eqs. (28) and (29) shows that fixing $N_{||} = 0$ results in $V_\alpha^{(12)} = V_\alpha^{(21)} = V_\alpha^{(13)} = V_\alpha^{(31)} = 0$. Moreover, a useful finding is that from the whole derivative,

$$\frac{\partial \mathbf{j}^{(n)}}{\partial k_\alpha} = \frac{c}{\omega}\left(\frac{K_\alpha}{K}\frac{\partial \mathbf{j}^{(n)}}{\partial N_\perp} + \frac{B_\alpha}{B}\frac{\partial \mathbf{j}^{(n)}}{\partial N_{||}}\right),$$

which is a part of the expression for $U_\alpha^{(mn)}$, only the term containing $B_\alpha$ will persist in the cases of $U_\alpha^{(12)}$, $U_\alpha^{(21)}$, $U_\alpha^{(13)}$, and $U_\alpha^{(31)}$. On the contrary, the term containing $K_\alpha$ is the only one that enters into $U_\alpha^{(23)}$ and $U_\alpha^{(32)}$. Next, at $N_{||} = 0$ the derivatives $\partial\lambda^{(m)}/\partial N_{||}$ vanish since all $\lambda^{(m)}$, in contrast to $\mathbf{j}^{(m)}$, depend solely on $N_{||}^2$. So in the calculation of $W_\pm^{(1)}$ the somewhat simplified expressions

$$\begin{aligned}\eta^{(1)} &= 2\frac{c}{\omega}\frac{\partial\left(\lambda_0^{(2)} - \lambda_0^{(1)}\right)}{\partial N_\perp}Q_{13}^{(2)}U_3^{(12)} \\ &\quad + \lambda_0^{(3)}U_3^{(13)}\left(V_3^{(32)} - 2Q_{13}^{(2)}U_1^{(32)}\right), \\ \eta^{(2)} &= 2\frac{c}{\omega}\frac{\partial\left(\lambda_0^{(1)} - \lambda_0^{(2)}\right)}{\partial N_\perp}Q_{13}^{(1)}U_3^{(21)} \\ &\quad - \lambda_0^{(3)}U_3^{(31)}\left(V_3^{(23)} + 2Q_{13}^{(1)}U_1^{(23)}\right),\end{aligned} \tag{31}$$

are actually involved, where

$$Q_{13}^{(m)} = 2\mu\sqrt{u}\frac{\omega}{c}\frac{\partial B}{B\partial r_3}\frac{\partial \mathrm{Re}\lambda_0^{(m)}}{\partial \xi_{-2}}\left(\frac{\partial \mathrm{Re}\lambda_0^{(m)}}{\partial N_\perp}\right)^{-1}. \tag{32}$$

Based on the above analysis, two important and not evident *a priori* statements should be made. (i) The single inhomogeneity parameter that defines the power exchange rate is the dimensionless longitudinal magnetic steepness $\Gamma \equiv (c/\omega)\mathbf{B}\cdot\nabla B/B^2$ in the BZ. In the plasma core of different toroidal devices, this parameter may range in magnitude from almost 0 (in tokamaks or torsatrons/heliotrons) to about $10^{-4}$ in heliac-type stellarators, while in magnetic mirror devices it may be much larger. (ii) For the effect under study, neither the microwave beam width nor the wave-front curvature affects the power exchange between $X$ and $O$ mode waves. It is precisely this fact that justifies extension of the results below to wave fields of forms other than the Gaussian beam.

Each cycle of numerical integration of Eqs. (24) and (25) was performed at constant $q$ and $\mu$, starting from the lower of two $u$ values at which the dispersion surfaces of both modes intersect [cf. Fig. 1(b)], in the direction of magnetic field increase, until the mode coherence breaks down. The initial amplitude of the $X$ mode was set to 1. Figure 2 shows the contours of the $O$ mode amplitude beyond the BZ in the most interesting ranges of $q$ and $\mu$ (here $T_e$ varies between ~1 keV at the bottom and ~0.1 keV at the top). In magnetic confinement fusion research, electron temperatures above several

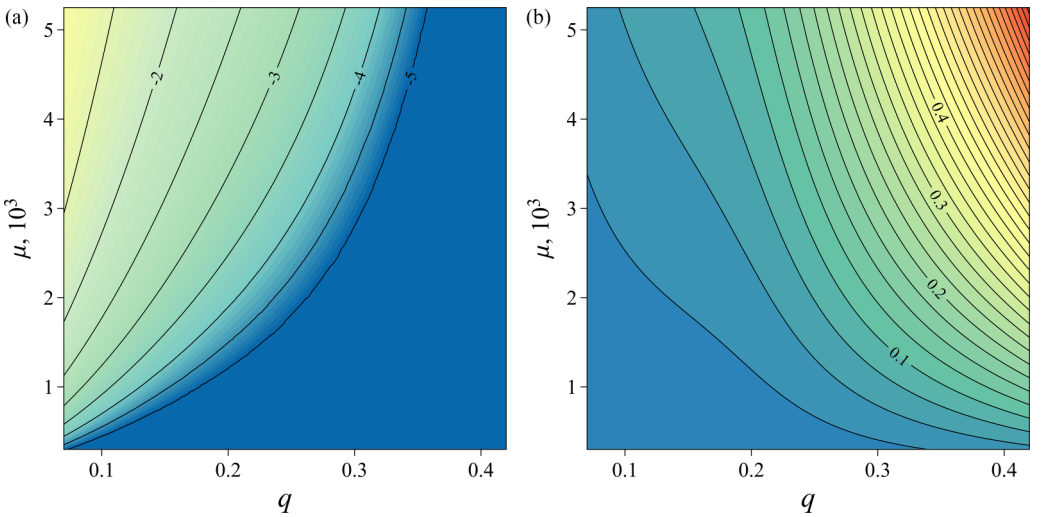


FIG. 3. (a) Relative amplitude of the unabsorbed $X$ mode (in decimal logarithm units; contours below $-5$ are not shown) beyond the BZ, without $X$-to-$O$ mode power transfer. (b) The magnitude of $\eta^{(1)}$ at the BZ boundary for $\Gamma = 2 \times 10^{-4}$.

hundred eV are typical for ECRH operating regimes, while lower temperatures may be of interest to special regimes or plasma technology. We intentionally excluded the plasma-vacuum interface limit $q \to 0$ because in the given numerical model it would correspond to an unphysical infinitely long BZ. We also excluded the $X$ mode cutoff limit $q \to 0.5$ in view of what has been stated above.

It can be seen from Fig. 2 that roughly at $T_e > 200$ eV a very small fraction of the arriving $X$ mode power is transferred to the $O$ mode even at the maximum magnitudes of $\Gamma$ that may occur in toroidal devices near the magnetic axis (for example, in the TJ-II stellarator). Almost all the remaining power is absorbed within the BZ. It is also noticeable that the overall power transfer exhibits a nonmonotonic dependence on $q$, that is on plasma density. This effect can be explained by comparing the distributions presented in Figs. 3(a) and 3(b). The magnitude of $\eta^{(1)}$, which characterizes the power exchange rate, increases along with $q$. However, in the range $q < 0.2$, fast reduction of the $\mathrm{Im}\lambda^{(2)}$ peak magnitude towards lower values of $q$ [cf. also Fig. 1(d)] prevents an abrupt complete absorption of the $X$ mode within the BZ, thus extending the power exchange zone.

One should note that, under typical conditions of second harmonic ECRH, the requirement $|\mathrm{Im}\lambda^{(2)}| \ll 1$ of the weakly inhomogeneous approximation is only marginally satisfied in the resonance region. Therefore, it would be of interest to compare the presented results, which are based on asymptotic consideration, with the results of 3D full-wave modeling, if the corresponding codes will ever incorporate finite-temperature effects.

## V. SUMMARY

In this paper, we have extended the short-wavelength paraxial asymptotic technique, widely known as Gaussian beam tracing, to the case of two interacting modes in non-Hermitian plasmas. This is an interesting analytical problem *per se* but is also practically important since such a situation often takes place in second harmonic ECRH schemes: if the wave propagates perpendicularly to the magnetic field, $X$ and $O$ mode waves are linearly coupled near the resonance. The theoretical outcome of our study is a system of ordinary differential equations, which contains two amplitude equations of the form of Eq. (24) and the phase difference equation in Eq. (25). In a hierarchy of computation, these equations are appended to the basic system of beam tracing equations. However, the problem under consideration does not require the full-scale use of a beam tracing code, because the spatial distribution of the wave field is beyond what we need to know. The particular parameters for second harmonic ECRH of all the equations involved are implicitly given by the expressions obtained in Sec. III. A detailed analysis of the parameters responsible for power transfer between $X$ and $O$ mode waves has shown the following. Among the different inhomogeneities that may occur in magnetically confined plasmas, only the longitudinal steepness of the magnetic field in the BZ affects the power transfer rate. In addition, the latter is affected by neither the microwave beam width nor the wave-front curvature. Since any microwave spatial distribution can be decomposed into a sum of independent Gaussian beamlets with adjustable parameters [18], the paraxial approximation adopted initially does not reduce the generality of results.

Numerical integration of the obtained equations was performed systematically for the strictly perpendicular propagation case. It was found that the power fraction, which is eventually transferred to the weakly absorbed $O$ mode, is expected to be very small in toroidal devices at electron temperatures above $\sim$200 eV. The main reason for the low overall efficiency of $X$-to-$O$ mode power transfer is very fast resonant absorption of the $X$ mode wave in the BZ. Thus, the effect of non-Hermitian mode coupling near the resonance cannot impair ECRH in most experimental setups, with the exception of magnetic mirror systems. However, during the initial phase of ECRH plasma startup, it may somewhat worsen the performance.

All data that support the findings of this study are included within the article.

## ACKNOWLEDGMENTS

This study was carried out under State Task No. 0024-2019-0006 of the Ministry of Science and Higher Education of the Russian Federation, "Physics of high-temperature plasma. Fundamental problems of plasma dynamics, confinement and heating in three-dimensional magnetic configurations."


## APPENDIX A: DERIVATION OF EQ. (8)

Let us substitute Eqs. (6) and (7) into Eq. (1), replace $\mathbf{r}'$ by $\mathbf{r}-\boldsymbol{\rho}$, and change the order of integration to obtain $\int \exp(i\mathbf{k}\cdot\mathbf{r})\Sigma(\mathbf{k},\mathbf{r})d^3\mathbf{k}=\mathbf{0}$, where

$$\begin{aligned}\Sigma(\mathbf{k},\mathbf{r}) \equiv & \int\left(\mathbf{L}-\frac{\rho_\alpha}{2}\frac{\partial\mathbf{L}}{\partial r_\alpha}\right)\left(1-\rho_\beta\frac{\partial}{\partial r_\beta}+\frac{i}{2}\rho_\beta\rho_\gamma Q_{\beta\gamma}\right)\\ &\times\exp\left(-i\mathbf{k}\cdot\boldsymbol{\rho}\right)d^3\boldsymbol{\rho}\,\mathbf{A}(\mathbf{k},\mathbf{r})\\ =&\,\boldsymbol{\Lambda}\mathbf{A}-\frac{i}{2}\frac{\partial^2\boldsymbol{\Lambda}}{\partial k_\alpha\partial r_\alpha}\mathbf{A}-i\frac{\partial\boldsymbol{\Lambda}}{\partial k_\alpha}\frac{\partial\mathbf{A}}{\partial r_\alpha}-\frac{i}{2}\frac{\partial^2\boldsymbol{\Lambda}}{\partial k_\alpha\partial k_\beta}\mathbf{A}Q_{\alpha\beta}\\ &-\frac{1}{2}\frac{\partial^3\boldsymbol{\Lambda}}{\partial k_\alpha\partial r_\alpha\partial k_\beta}\frac{\partial\mathbf{A}}{\partial r_\beta}-\frac{1}{4}\frac{\partial^4\boldsymbol{\Lambda}}{\partial k_\alpha\partial r_\alpha\partial k_\beta\partial k_\gamma}\mathbf{A}Q_{\beta\gamma}.\end{aligned}\tag{A1}$$

Here $\boldsymbol{\Lambda}(\mathbf{k},\mathbf{r})\equiv\int\exp(-i\mathbf{k}\cdot\boldsymbol{\rho})\mathbf{L}(\boldsymbol{\rho},\mathbf{r})d^3\boldsymbol{\rho}$. The last two terms on the right-hand side of Eq. (A1) are the products of two quantities, each being relatively small, which is why we may neglect them. The condition $\Sigma=\mathbf{0}$ thus leads to Eq. (8).

## APPENDIX B: COMPLETE EXPRESSIONS FOR THE MATRICES IN EQ. (9)

Let us rewrite the first matrix of Eq. (9) in the form

$$\mathbf{G}_\alpha=\mathbf{X}^{-1}\frac{\partial(\mathbf{XD})}{\partial k_\alpha}-\mathbf{D}\mathbf{X}^{-1}\frac{\partial\mathbf{X}}{\partial k_\alpha},$$

then we obtain

$$\begin{aligned}G_{\alpha mn}&=\mathbf{y}^{(m)}\cdot\frac{\partial(\lambda^{(n)}\mathbf{x}^{(n)})}{\partial k_\alpha}-\lambda^{(m)}\mathbf{y}^{(m)}\cdot\frac{\partial\mathbf{x}^{(n)}}{\partial k_\alpha}\\&=I_{mn}\frac{\partial\lambda^{(n)}}{\partial k_\alpha}+(\lambda^{(n)}-\lambda^{(m)})U_\alpha^{(mn)}.\end{aligned}\tag{B1}$$

The second matrix may be represented as

$$\hat{\mathbf{G}}_{\alpha\beta}=\frac{\partial\mathbf{G}_\alpha}{\partial k_\beta}+\mathbf{X}^{-1}\frac{\partial\mathbf{X}}{\partial k_\beta}\mathbf{G}_\alpha-\mathbf{G}_\alpha\mathbf{X}^{-1}\frac{\partial\mathbf{X}}{\partial k_\beta},$$

which yields

$$\begin{aligned}\hat{G}_{\alpha\beta mn}&=\frac{\partial G_{\alpha mn}}{\partial k_\beta}+U_\beta^{(m\nu)}G_{\alpha\nu n}-G_{\alpha m\nu}U_\beta^{(\nu n)}\\&=I_{mn}\frac{\partial^2\lambda^{(n)}}{\partial k_\alpha\partial k_\beta}+(\lambda^{(n)}-\lambda^{(m)})\frac{\partial U_\alpha^{(mn)}}{\partial k_\beta}\\&\quad+\frac{\partial(\lambda^{(n)}-\lambda^{(m)})}{\partial k_\alpha}U_\beta^{(mn)}+\frac{\partial(\lambda^{(n)}-\lambda^{(m)})}{\partial k_\beta}U_\alpha^{(mn)}\\&\quad+(\lambda^{(m)}-\lambda^{(\nu)})U_\alpha^{(m\nu)}U_\beta^{(\nu n)}+(\lambda^{(n)}-\lambda^{(\nu)})U_\beta^{(m\nu)}U_\alpha^{(\nu n)}.\end{aligned}\tag{B2}$$

Similarly, we may write the third matrix as

$$\mathbf{F}=\mathbf{G}_\alpha\mathbf{X}^{-1}\frac{\partial\mathbf{X}}{\partial r_\alpha}+\mathbf{X}^{-1}\frac{\partial\mathbf{X}}{\partial r_\alpha}\mathbf{G}_\alpha,$$

and hence

$$\begin{aligned}F_{mn}&=G_{\alpha m\nu}V_\alpha^{(\nu n)}+V_\alpha^{(m\nu)}G_{\alpha\nu n}\\&=\frac{\partial(\lambda^{(m)}+\lambda^{(n)})}{\partial k_\alpha}V_\alpha^{(mn)}+(\lambda^{(\nu)}-\lambda^{(m)})U_\alpha^{(m\nu)}V_\alpha^{(\nu n)}\\&\quad+(\lambda^{(n)}-\lambda^{(\nu)})V_\alpha^{(m\nu)}U_\alpha^{(\nu n)}.\end{aligned}\tag{B3}$$


[1] M. Bornatici, R. Cano, O. De Barbieri, and F. Engelmann, Electron cyclotron emission and absorption in fusion plasmas, Nucl. Fusion **23**, 1153 (1983).

[2] A. D. Piliya and V. I. Fedorov, Electron cyclotron plasma heating in tokamaks, in *Reviews of Plasma Physics*, edited by B. B. Kadomtsev (Consultants Bureau, New York, London, 1987), Vol. 13, pp. 335–388.

[3] V. V. Alikaev, A. G. Litvak, E. V. Suvorov, and A. A. Fraiman, Electron cyclotron resonance heating of toroidal plasmas, in *High-frequency Plasma Heating*, edited by A. G. Litvak (American Institute of Physics, New York, 1992), pp. 1–64.

[4] V. Erckmann and U. Gasparino, Electron cyclotron resonance heating and current drive in toroidal fusion plasmas, Plasma Phys. Control. Fusion **36**, 1869 (1994).

[5] H. P. Laqua, J. Baldzuhn, H. Braune, S. Bozhenkov, K. Brunner *et al.*, High-performance ECRH at W7-X: Experience and perspectives, Nucl. Fusion **61**, 106005 (2021).

[6] D. Wagner, D. Schmid-Lorch, J. Stober, H. Höhnle, F. Leuterer *et al.*, Feed forward polarization control during ECRH discharges at ASDEX Upgrade, Fusion Sci. Technol. **58**, 658 (2010).

[7] A. I. Meshcheryakov, G. M. Batanov, V. D. Borzosekov, S. E. Grebenshchikov, I. A. Grishina *et al.*, Plasma confinement during ECR heating with a volume power density of 3 MW/m$^3$ at the L-2M stellarator, J. Phys.: Conf. Ser. **907**, 012016 (2017).

[8] Yu. N. Dnestrovskij, A. V. Danilov, A. Yu. Dnestrovskij, L. A. Klyuchnikov, S. E. Lysenko *et al.*, Comparison of plasma heating at first and second electron cyclotron harmonics in the T-10 tokamak, Plasma Phys. Rep. **46**, 477 (2020).

[9] M. A. Tereshchenko, Decrease in the mode purity of microwave beams in the L-2M stellarator peripheral plasma, Bull. Lebedev Phys. Inst. **47**, 399 (2020).

[10] E. Z. Gusakov and A. Yu. Popov, Possible transition from modest to strong anomalous absorption in X2-mode electron cyclotron resonance heating experiments in toroidal devices, Plasma Phys. Control. Fusion **62**, 025028 (2020).

[11] A. B. Altukhov, V. I. Arkhipenko, A. D. Gurchenko, E. Z. Gusakov, A. Yu. Popov, L. V. Simonchik, and M. S. Usachonak, Observation of the strong anomalous absorption of the X-mode pump in a plasma filament due to the two-plasmon decay, Europhys. Lett. **126**, 15002 (2019).

[12] S. K. Hansen, A. S. Jacobsen, M. Willensdorfer, S. K. Nielsen, J. Stober *et al.*, Microwave diagnostics damage by parametric decay instabilities during electron cyclotron resonance heating in ASDEX Upgrade, Plasma Phys. Control. Fusion **63**, 095002 (2021).

[13] E. R. Tracy, A. J. Brizard, A. S. Richardson, and A. N. Kaufman, *Ray Tracing And Beyond: Phase Space Methods in Plasma Wave Theory* (Cambridge University Press, Cambridge, New York, 2014).

[14] I. Y. Dodin, D. E. Ruiz, K. Yanagihara, Y. Zhou, and S. Kubo, Quasioptical modeling of wave beams with and without mode conversion. I. Basic theory, Phys. Plasmas **26**, 072110 (2019).

[15] S. W. McDonald, Phase-space Eikonal Method for Treating Wave Equations, Phys. Rev. Lett. **54**, 1211 (1985).

[16] M. Tereshchenko, F. Castejón, S. Pavlov, and Á. Cappa, Power-flow formulation of a ray approach to the modelling of inhomogeneous waves, Phys. Scr. **84**, 025401 (2011).

[17] P. F. Goldsmith, *Quasioptical Systems: Gaussian Beam Quasioptical Propagation and Applications* (IEEE, New York, 1998).

[18] M. Tereshchenko, F. Castejón, and Á. Cappa, Application of Gabor expansion to beam-tracing problems in inhomogeneous plasmas, Plasma Phys. Control. Fusion **55**, 115011 (2013).

[19] Y. Ashida, Z. Gong, and M. Ueda, Non-Hermitian physics, Adv. Phys. **69**, 249 (2020).

[20] S. Feng and H. G. Winful, Physical origin of the Gouy phase shift, Opt. Lett. **26**, 485 (2001).

[21] W. D. Hayes, Kinematic wave theory, Proc. R. Soc. London, Ser. A **320**, 209 (1970).

[22] I. B. Bernstein, Geometric optics in space- and time-varying plasmas, Phys. Fluids **18**, 320 (1975).

[23] G. V. Pereverzev, Beam tracing in inhomogeneous anisotropic plasmas, Phys. Plasmas **5**, 3529 (1998).

[24] E. Poli, A. G. Peeters, and G. V. Pereverzev, TORBEAM, a beam tracing code for electron-cyclotron waves in tokamak plasmas, Comput. Phys. Commun. **136**, 90 (2001).

[25] M. A. Tereshchenko, Propagation of microwave beams through the stagnation zone in an inhomogeneous plasma, Plasma Phys. Rep. **43**, 18 (2017).

[26] R. G. Littlejohn and W. G. Flynn, Geometric phases in the asymptotic theory of coupled wave equations, Phys. Rev. A **44**, 5239 (1991).

[27] M. A. Tereshchenko, Microwave beam bifurcation in an inhomogeneous plasma: Modeling by ray methods, Plasma Phys. Rep. **46**, 740 (2020).

[28] V. V. Zheleznyakov, V. V. Kocharovskii, and Vl. V. Kocharovskii, Linear coupling of electromagnetic waves in inhomogeneous weakly-ionized media, Sov. Phys. Usp. **26**, 877 (1983).

[29] Yu. A. Kravtsov, O. N. Naida, and A. A. Fuki, Waves in weakly anisotropic 3D inhomogeneous media: Quasi-isotropic approximation of geometrical optics, Phys. Usp. **39**, 129 (1996).

[30] I. P. Shkarofsky, Dielectric tensor in Vlasov plasmas near cyclotron harmonics, Phys. Fluids **9**, 561 (1966).

[31] V. Krivenski and A. Orefice, Weakly relativistic dielectric tensor and dispersion functions of a Maxwellian plasma, J. Plasma Phys. **30**, 125 (1983).

[32] F. Castejón, Á. Cappa, M. Tereshchenko, S. S. Pavlov, and Á. Fernández, Weakly relativistic and nonrelativistic estimates of EBW heating in the TJ-II stellarator, Fusion Sci. Technol. **52**, 230 (2007).

[33] F. Castejón, Á. Cappa, M. Tereshchenko, and Á. Fernández, Computation of EBW heating in the TJ-II stellarator, Nucl. Fusion **48**, 075011 (2008).

[34] D. Farina, Relativistic dispersion relation of electron cyclotron waves, Fusion Sci. Technol. **53**, 130 (2008).